JACS
JOURNAL OF THE AMERICAN CHEMICAL SOCIETY
Cite This: J. Am. Chem. Soc. 2019, 141, 19241−19245
Communication
pubs.acs.org/JACS

Cobalt-Based Nitride-Core Oxide-Shell Oxygen Reduction Electrocatalysts

Yao Yang,[†] Rui Zeng,[†] Yin Xiong, Francis J. DiSalvo, and Héctor D. Abruña*

Department of Chemistry and Chemical Biology, Baker Laboratory, Cornell University, Ithaca, New York 14853, United States

Supporting Information

ABSTRACT: Developing high-performance, low-cost, and conductive nonprecious electrocatalysts for the oxygen reduction reaction (ORR) has been a key challenge for advancing fuel cell technologies. Here, we report on a novel family of cobalt nitrides (Co_xN/C, x = 2, 3, 4) as ORR electrocatalysts in alkaline fuel cells. Co_4N/C exhibited the highest ORR activity among the three types of cobalt nitrides studied, with a half-wave potential ($E_{1/2}$) of 0.875 V vs RHE in 1 M KOH, rivaling that of commercial Pt/C (0.89 V). Moreover, Co_4N/C showed an 8-fold improvement in mass activity at 0.85 V, when compared to cobalt oxide, Co_3O_4/C, and a negligible degradation ($\Delta E_{1/2}$ = 14 mV) after 10 000 potential cycles. The superior performance was ascribed to the formation of a conductive nitride core surrounded by a naturally formed thin oxide shell (about 2 nm). The conductive nitride core effectively mitigated the low conductivity of the metal oxide, and the thin oxide shell on the surface provided the active sites for the ORR. Strategies developed herein represent a promising approach for the design of other novel metal nitrides as electrocatalysts for fuel cells.

Hydrogen fuel cells represent one of the most promising renewable energy technologies for electric vehicles due to their high energy conversion efficiency.[1,2] However, the sluggish oxygen reduction reaction (ORR) has precluded the broad deployment of fuel cell technologies.[3−5] Proton exchange membrane fuel cells (PEMFCs) require significant amounts of Pt-based catalysts to facilitate the ORR for high power density applications (1 W/cm^2).[2,6,7] Alternatively, alkaline fuel cells enable the use of nonprecious metal catalysts, such as transition metals and oxides, as they are much more stable in alkaline media.[8] A variety of nonprecious-metal-containing catalysts have been explored, including Fe/Co−N−C,[9,10] perovskites,[11] transition metal oxides,[12−15] phosphides,[16] and nitrides.[17−19] Among them, metal oxides, especially spinel oxides, have drawn considerable attention due to their superior activities.[8,20,21] However, bulk metal oxides, like Co_3O_4, have a low intrinsic electronic conductivity due to their large band gap (>2 eV) and small nanoparticles only partially mitigate their insulating character.[22,23] It is thus important to develop novel conductive metal-based catalysts for the ORR. Benefiting from their conductive nature and, often, metallic behavior,[24] transition metal nitrides have emerged as a new family of ORR electrocatalysts. Previous reports include early 3d metal nitrides,[25] Mn-,[19] Fe-,[26] Co-,[18] and Ni-based nitrides,[27,28] Cu_3N,[17,29] MoN,[18] and other bimetallic nitrides.[18,25] However, the reported activities are at best modest ($E_{1/2}$ < 0.8 V vs reversible hydrogen electrode, RHE) and generally far lower than that of Pt/C (Table S1). Cobalt-based nitrides have been reported to exhibit promising performance in water splitting,[24,30−32] metal-air batteries,[33,34] and supercapacitors.[35]

Here, we have prepared a series of cobalt nitrides loaded on carbon supports by a facile nitridation process in NH_3. The crystal structures of the as-synthesized cobalt nitrides were characterized by powder X-ray diffraction (XRD) (Figures 1a and S1). The XRD patterns of Co_2N/C, Co_3N/C, and Co_4N/C matched well with those of standard references, Co_2N (PDF 04-004-4638), Co_3N (PDF 04-021-6263), and Co_4N (PDF 04-021-6262), respectively, indicating a successful synthesis of single-phase cobalt nitrides. This finding highlights the key role of the synthesis temperature in determining the Co/N ratio. As shown in Figure 1b, increases in the temperature led to a monotonic increase of the Co/N ratio, indicating a gradual loss of nitrogen from the cobalt nitride crystals at higher temperatures. The characteristic temperatures for the formation of Co_2N, Co_3N, and Co_4N were 300, 360, and 460 °C,

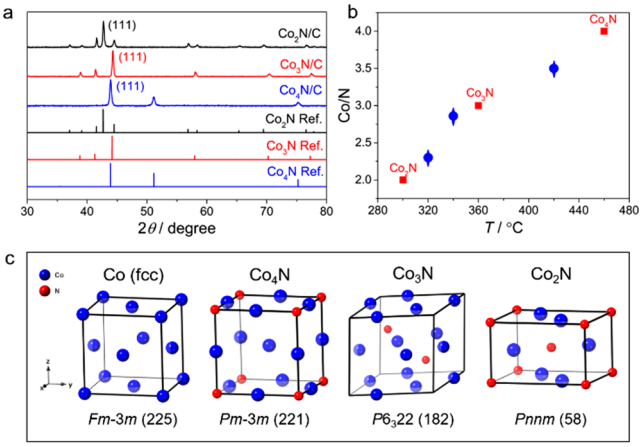

Figure 1. (a) XRD patterns of Co_2N/C, Co_3N/C, and Co_4N/C and the corresponding standard XRD references. (b) Co/N atomic ratio vs synthesis temperature. Red marks indicate the single phase Co_xN/C materials while blue marks suggest mixed phases. (c) Crystal models of Co, Co_4N, Co_3N, and Co_2N.

Received: October 8, 2019
Published: November 19, 2019

DOI: 10.1021/jacs.9b10809
J. Am. Chem. Soc. 2019, 141, 19241−19245

respectively, as indicated by the red marks in Figure 1b. Mixed phases would coexist when the annealing temperatures were in between the aforementioned characteristic temperatures (blue marks in Figure 1b). We propose the following temperature effects during NH_3 treatment: the precursor is directly reduced by ammonia to Co_2N at 300 °C; further temperature increases lead to the partial decomposition of Co_2N, giving rise to Co_3N at 360 °C and further decomposition yielding Co_4N at 460 °C. From the perspective of crystal structures (Figure 1c), Co_4N exhibits a similar cubic structure to the cubic metallic Co and both show similar XRD patterns with just slight differences in *d*-spacings (Figure S1g). Further incorporation of N atoms into the lattice induces the transformation to new crystal structures. While Co_3N adopts a hexagonal structure with six cobalt and two nitrogen atoms in the unit cell, Co_2N exhibits an orthorhombic structure with a much lower symmetry.

The microstructure of the as-synthesized Co_4N/C was examined, at the atomic scale, using an aberration-corrected high-angle annular dark-field (HAADF) scanning transmission electron microscope (STEM) equipped with an electron energy loss spectrometer (EELS). Atomic-scale TEM images suggested *d*-spacings of 2.1 Å, consistent with the theoretical values of (111) facets of Co_4N (Figure S2). The chemical compositions of Co_4N NPs were investigated using EELS analysis (Figure 2), which was obtained from the Co $L_{3,2}$ edges

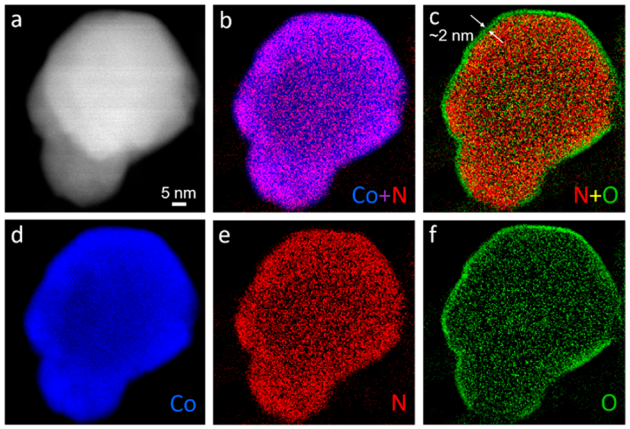

Figure 2. STEM-EELS analysis of the nitride-core and oxide-shell of Co_4N/C. (a) HAADF-STEM image of one Co_4N nanoparticle. (b–f) The corresponding EELS elemental maps of Co in green (d), N in red (e), O in green (f), and composite maps of Co vs N (b) and O vs N (c), respectively.

and N K-edge (Figure S3). The as-synthesized Co_4N NPs exhibited a relatively homogeneous elemental distribution of Co and N, which confirmed the uniform incorporation of N through the nanoparticles. Surprisingly, a pronounced O K-edge emerged in the EELS spectrum (Figure S3) and resulted in an O elemental map with clear surface enrichment (Figure 2f). The composite map of O vs N suggested a thin oxygen shell on the surface with a uniform thickness of about 2 nm (i.e., ~6 atomic layers, Figures 2 and S4). In an effort to further distinguish the chemical environment of the nitride core from the surface oxide layer, electron energy-loss near-edge structure (ELNES) analysis was employed to study the Co $L_{3,2}$ edges at the single-nanoparticle level with a high energy resolution of 0.5 eV. The ELNES spectrum of the nitride core exhibited a lower edge energy than the oxide shell (Figure S5), which is likely due to the average Co valence in the nitride core being lower than in the oxide shell, consistent with previous X-ray absorption spectroscopy measurements.[36−39] The nitride core also exhibited a higher intensity ratio of L_2 to L_3 than that of the oxide shell, suggesting a relatively more covalent bonding for Co in the core.[38,39] This intriguing finding indicated that the as-synthesized Co_4N NPs would naturally form a thin surface layer of cobalt oxide, upon exposure to air. Such a "native oxide layer" is also known as a passivation layer with a thickness of several atomic layers, which can prevent further oxidation and is particularly common in aluminum.[40]

To elucidate the near-surface chemical environment, surface-sensitive X-ray photoelectron spectroscopy (XPS) was employed to study the surface oxide layer and near-surface nitride. Pronounced N and O 1s and Co 2p peaks appeared in the full XPS spectrum, indicating the presence of both cobalt nitride and oxide (Figure 3a). The higher intensity of the O 1s

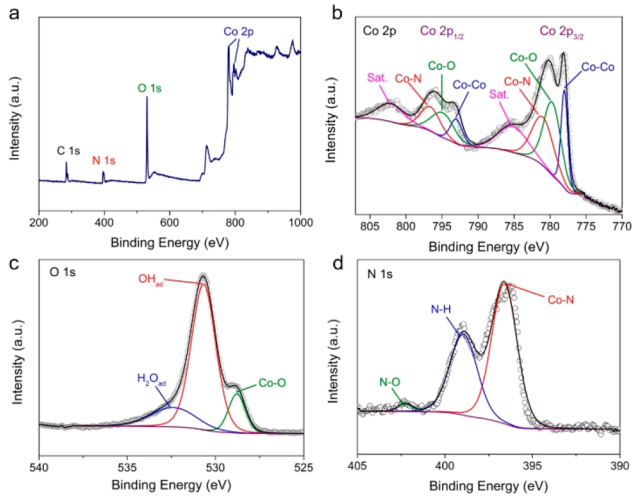

Figure 3. XPS spectra for Co_4N. (a) full spectrum. (b–d) High-resolution spectra of (b) Co 2p, (c) O 1s, and (d) N 1s.

peak, relative to the N 1s peak, is consistent with previous findings of the 2 nm surface oxide layer since the XPS penetration depth is ~5 nm. In the Co 2p spectrum (Figure 3b), the peaks at 778.0 and 793.0 eV were ascribed to the Co $2p_{3/2}$ and Co $2p_{1/2}$ of Co−Co coordination. The binding energies of 781 and 796.6 eV, corresponding to Co−N bonds, confirmed the formation of Co_4N after the nitridation process. The coexistence of both Co−Co and Co−N suggests two distinct chemical environments of Co in the Co_4N crystal structures with the Co atoms having nearest neighbors of two N atoms in a collinear geometry and 12 surrounding Co atoms (Figure 1c). The Co−O bond was evidenced by peaks located at 779.7 and 794.9 eV and further verified by the presence of Co−O coordination at 528.8 eV in the O 1s spectrum (Figure 3c). Besides the Co−O bond, from the surface cobalt oxide shell, a significant amount of OH and H_2O adsorbed on the surface were evident and identified by their distinct chemical shifts at 530.7 and 532.1 eV, respectively. In a previous report, we found that Co−OH_{ad} and Co−OH_{2ad} were able to activate water molecules on the surface and facilitate oxygen reduction.[20] Apart from the Co−N bond in Co_4N (396.1 eV), the peak at 399.0 eV in the N 1s spectrum could originate from the N−H surface terminal group after NH_3 treatment[41,42] while the binding energy of 402.0 eV was assigned to the formation of N−O interactions[43] at the interface between

DOI: 10.1021/jacs.9b10809
J. Am. Chem. Soc. 2019, 141, 19241−19245

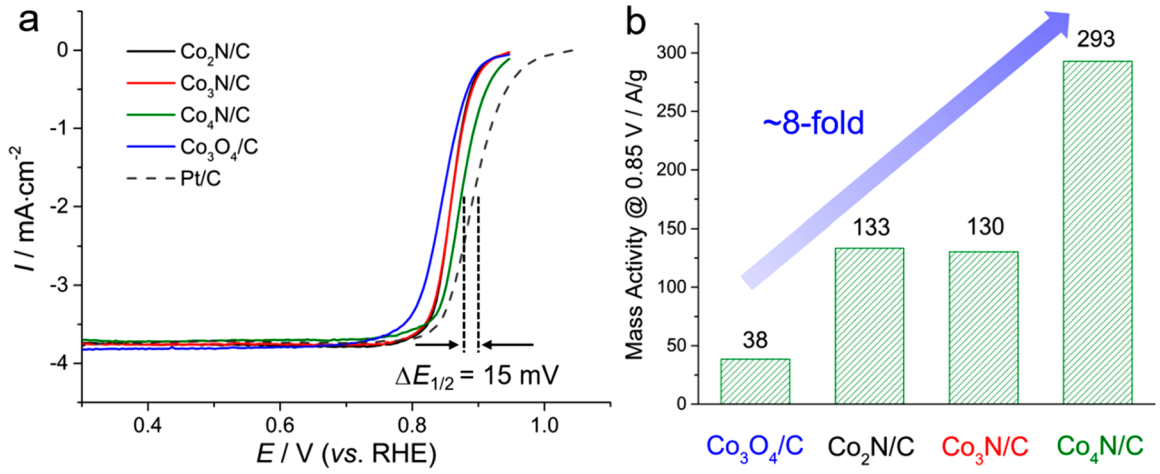

Figure 4. Evaluation of ORR activity of Co_xN/C. (a) ORR polarization profiles of Co_2N/C, Co_3N/C, Co_4N/C, Co_3O_4/C, and Pt/C in O_2-saturated 1 M KOH at 5 mV/s and 1600 rpm. (b) Mass activity (MA) of Co_2N/C, Co_3N/C, Co_4N/C, and Co_3O_4/C at 0.85 V vs RHE (normalized to the mass of Co).

cobalt oxide and Co_4N (Figure 3d). The combination of a conductive cobalt nitride core and an active cobalt oxide shell may serve as a rational design metric of heterogeneous structures to mitigate the low conductivity of metal oxides, yet remain as active sites on the surface, and work as promising ORR electrocatalysts.

The oxygen reduction activity of cobalt nitrides was evaluated with a rotating disk electrode (RDE) system (Figures 4a and S6). All the catalysts displayed a similar diffusion-limiting current of about -3.8 mA/cm^2 in 1 M KOH solution (Figure 4a), indicating a nearly four-electron ORR process, consistent with rotating ring disk electrode (RRDE) measurements (Figure S7). Based on the Levich equation, the I_d of the 4e$^-$ ORR in 0.1 M O_2-saturated KOH is -5.5 mA/cm^2 at 1600 rpm. However, the O_2 concentration (C_{O2}) in 1 M KOH at 25 °C and 1 atm is 8.42×10^{-4} mol/L, which is ~70% of the C_{O2} in 0.1 M KOH (1.21×10^{-3} mol/L),[44] so that the I_d of the 4e$^-$ ORR in 1 M KOH at 1600 rpm will be correspondingly lower with a value of -3.8 mA/cm^2. While Co_3O_4/C exhibited a high $E_{1/2}$ value of 0.845 V, both Co_2N/C and Co_3N/C outperformed the spinel oxide by 15 mV in $E_{1/2}$, suggesting enhanced ORR kinetics. Surprisingly, Co_4N/C achieved a further activity enhancement with an $E_{1/2}$ at 0.875 V, comparable to that of Pt/C (0.890 V), and the highest recorded performance when compared to other reports in the literature (Table S1). The enhanced activity was further evaluated in terms of the mass activity (MA) at 0.85 V vs RHE (Figure 4b). Compared to Co_3O_4/C, a significant 3-fold enhancement was observed for Co_2N/C and Co_3N/C. Furthermore, Co_4N/C reached a remarkable MA of ~300 A/g, respectively, representing an 8-fold increase when compared to Co_3O_4/C and much higher than other reports (Table S1). Co_4N/C exhibited a smaller Tafel slope of 49 mV/dec, relative to Pt/C (66 mV/dec, Figure S8). The enhanced ORR performance was attributed to the unique nitride-core oxide-shell structure, consistent with previous theoretical predictions.[45]

The stability of Co_4N/C was assessed by potential cycling between 0.60 and 0.95 V for 10 000 cycles. Co_4N/C exhibited significant stability with an $E_{1/2}$ decay of only 14 mV (Figure S9), close to that of Pt/C (17 mV) (Figure S10). Given that the synthesis involved the NH_3 treatment of Co precursors on carbon supports, it appears plausible that Co-containing N-doped carbon (Co−N−C) structures possibly formed and might contribute to the observed catalytic enhancement since Co−N−C based materials are known to be active sites for the ORR.[46,47] Even though no evidence of single Co atoms on carbon was observed in STEM imaging, in order to rigorously evaluate such a possibility, we carried out acid wash experiments to remove Co_4N by treating Co_4N/C in hot H_2SO_4. The absence of the characteristic XRD peaks of Co_4N indicated that Co_4N was completely removed after acid treatment (Figure S11a). As a result, the removal of Co_4N led to a severe degradation of ORR performance with a negative shift of $E_{1/2}$ by >50 mV (Figure S11b). This dramatic activity loss suggested that Co_4N, rather than the possible existence of Co−N−C, played a key role in determining the ORR activity of Co_4N/C. Additionally, a mechanical mixture of Co_4N and carbon exhibited enhanced performance compared to the NH_3-treated carbon support (Figure S12), again confirming the high electrocatalytic activity of Co_4N. However, this improvement was still far inferior to the synthesized Co_4N/C by ~50 mV in terms of $E_{1/2}$, which suggested the importance of intimate interactions, during the one-pot synthesis between active materials and carbon supports.

In summary, Co_xN/C were successfully prepared by nitridation. These materials displayed significantly enhanced ORR activity, with Co_4N/C achieving an activity and durability comparable to those of Pt/C. This remarkable performance was mainly attributed to the formation of a conductive nitride-core active oxide-shell structure. Our work may shed light upon the development of new transition metal nitrides not only for alkaline fuel cells but also for other renewable energy technologies, in general.

■ ASSOCIATED CONTENT

Supporting Information

The Supporting Information is available free of charge at https://pubs.acs.org/doi/10.1021/jacs.9b10809.

Synthesis, structural characterizations of XRD, S/TEM, EELS and XPS, and electrochemical tests, including Table S1 and Figures S1−S12 (PDF)

DOI: 10.1021/jacs.9b10809
J. Am. Chem. Soc. 2019, 141, 19241−19245

AUTHOR INFORMATION

Corresponding Author

*hda1@cornell.edu

ORCID

Yao Yang: 0000-0003-0321-3792
Rui Zeng: 0000-0002-7577-767X
Héctor D. Abruña: 0000-0002-3948-356X

Author Contributions

†Y.Y. and R.Z. contributed equally to this work.

Notes

The authors declare no competing financial interest.

ACKNOWLEDGMENTS

This work was primarily supported by the Center for Alkaline-Based Energy Solutions (CABES), part of the Energy Frontier Research Center (EFRC) program supported by the U.S. Department of Energy, under Grant DE-SC-0019445. This work made use of TEM facilities at the Cornell Center for Materials Research (CCMR) which are supported through the National Science Foundation Materials Research Science and Engineering Center (NSF MRSEC) program (DMR-1719875). We are grateful to Malcolm (Mick) Thomas at CCMR for the help in Nion UltraSTEM.

REFERENCES

(1) Debe, M. K. Electrocatalyst Approaches and Challenges for Automotive Fuel Cells. *Nature* **2012**, *486*, 43−51.

(2) Gasteiger, H. A.; Kocha, S. S.; Sompalli, B.; Wagner, F. T. Activity Benchmarks and Requirements for Pt, Pt-Alloy, and Non-Pt Oxygen Reduction Catalysts for PEMFCs. *Appl. Catal., B* **2005**, *56*, 9−35.

(3) Wang, D.; Xin, H. L.; Hovden, R.; Wang, H.; Yu, Y.; Muller, D. A.; Disalvo, F. J.; Abruña, H. D. Structurally Ordered Intermetallic Platinum-Cobalt Core-Shell Nanoparticles with Enhanced Activity and Stability as Oxygen Reduction Electrocatalysts. *Nat. Mater.* **2013**, *12*, 81−87.

(4) Xiong, Y.; Yang, Y.; Joress, H.; Padgett, E.; Gupta, U.; Yarlagadda, V.; Agyeman-Budu, D. N.; Huang, X.; Moylan, T. E.; Zeng, R.; Kongkanand, A.; Escobedo, F. A.; Brock, J. D.; DiSalvo, F. J.; Muller, D. A.; Abruña, H. D. Revealing the Atomic Ordering of Binary Intermetallics Using in Situ Heating Techniques at Multilength Scales. *Proc. Natl. Acad. Sci. U. S. A.* **2019**, *116*, 1974−1983.

(5) Chung, H. T.; Cullen, D. A.; Higgins, D.; Sneed, B. T.; Holby, E. F.; More, K. L.; Zelenay, P. Direct Atomic-Level Insight into the Active Sites of a High-Performance PGM-Free ORR Catalyst. *Science* **2017**, *357*, 479−484.

(6) Xiong, Y.; Yang, Y.; DiSalvo, F. J.; Abruña, H. D. Pt-Decorated Composition-Tunable Pd−Fe@Pd/C Core−Shell Nanoparticles with Enhanced Electrocatalytic Activity toward the Oxygen Reduction Reaction. *J. Am. Chem. Soc.* **2018**, *140*, 7248−7255.

(7) Stamenkovic, V. R.; Strmcnik, D.; Lopes, P. P.; Markovic, N. M. Energy and Fuels from Electrochemical Interfaces. *Nat. Mater.* **2017**, *16*, 57−69.

(8) Zhao, Q.; Yan, Z.; Chen, C.; Chen, J. Spinels: Controlled Preparation, Oxygen Reduction/Evolution Reaction Application, and Beyond. *Chem. Rev.* **2017**, *117*, 10121−10211.

(9) Zitolo, A.; Goellner, V.; Armel, V.; Sougrati, M.-T.; Mineva, T.; Stievano, L.; Fonda, E.; Jaouen, F. Identification of Catalytic Sites for Oxygen Reduction in Iron- and Nitrogen-Doped Graphene Materials. *Nat. Mater.* **2015**, *14*, 937−942.

(10) Rojas-Carbonell, S.; Artyushkova, K.; Serov, A.; Santoro, C.; Matanovic, I.; Atanassov, P. Effect of PH on the Activity of Platinum Group Metal-Free Catalysts in Oxygen Reduction Reaction. *ACS Catal.* **2018**, *8*, 3041−3053.

(11) Suntivich, J.; Gasteiger, H. A.; Yabuuchi, N.; Nakanishi, H.; Goodenough, J. B.; Shao-Horn, Y. Design Principles for Oxygen-Reduction Activity on Perovskite Oxide Catalysts for Fuel Cells and Metal−Air Batteries. *Nat. Chem.* **2011**, *3*, 546−550.

(12) Yang, Y.; Xiong, Y.; Holtz, M. E.; Feng, X.; Zeng, R.; Chen, G.; Muller, D. A.; Abruña, H. D.; DiSalvo, F. J. Octahedral Spinel Electrocatalysts for Alkaline Fuel Cells. *Proc. Natl. Acad. Sci. U. S. A.* **2019**, 201906570.

(13) Indra, A.; Menezes, P. W.; Sahraie, N. R.; Bergmann, A.; Das, C.; Tallarida, M.; Schmeißer, D.; Strasser, P.; Driess, M. Unification of Catalytic Water Oxidation and Oxygen Reduction Reactions: Amorphous Beat Crystalline Cobalt Iron Oxides. *J. Am. Chem. Soc.* **2014**, *136*, 17530−17536.

(14) Liang, Y.; Li, Y.; Wang, H.; Zhou, J.; Wang, J.; Regier, T.; Dai, H. Co_3O_4 Nanocrystals on Graphene as a Synergistic Catalyst for Oxygen Reduction Reaction. *Nat. Mater.* **2011**, *10*, 780−786.

(15) Xiong, Y.; Yang, Y.; Feng, X.; DiSalvo, F. J.; Abruña, H. D. A Strategy for Increasing the Efficiency of the Oxygen Reduction Reaction in Mn-Doped Cobalt Ferrites. *J. Am. Chem. Soc.* **2019**, *141*, 4412−4421.

(16) Yang, H.; Zhang, Y.; Hu, F.; Wang, Q. Urchin-like CoP Nanocrystals as Hydrogen Evolution Reaction and Oxygen Reduction Reaction Dual-Electrocatalyst with Superior Stability. *Nano Lett.* **2015**, *15*, 7616−7620.

(17) Wu, H.; Chen, W. Copper Nitride Nanocubes: Size-Controlled Synthesis and Application as Cathode Catalyst in Alkaline Fuel Cells. *J. Am. Chem. Soc.* **2011**, *133*, 15236−15239.

(18) Cao, B.; Veith, G. M.; Diaz, R. E.; Liu, J.; Stach, E. A.; Adzic, R. R.; Khalifah, P. G. Cobalt Molybdenum Oxynitrides: Synthesis, Structural Characterization, and Catalytic Activity for the Oxygen Reduction Reaction. *Angew. Chem., Int. Ed.* **2013**, *52*, 10753−10757.

(19) Miura, A.; Rosero-Navarro, C.; Masubuchi, Y.; Higuchi, M.; Kikkawa, S.; Tadanaga, K. Nitrogen-Rich Manganese Oxynitrides with Enhanced Catalytic Activity in the Oxygen Reduction Reaction. *Angew. Chem., Int. Ed.* **2016**, *55*, 7963−7967.

(20) Wang, Y.; Yang, Y.; Jia, S.; Wang, X.; Lyu, K.; Peng, Y.; Zheng, H.; Wei, X.; Ren, H.; Xiao, L.; Wang, J.; Muller, D. A.; Abruña, H. D.; Hwang, B. J.; Lu, J.; Zhuang, L. Synergistic Mn-Co Catalyst Outperforms Pt on High-Rate Oxygen Reduction for Alkaline Polymer Electrolyte Fuel Cells. *Nat. Commun.* **2019**, *10*, 1506.

(21) Yang, Y.; Wang, Y.; Xiong, Y.; Huang, X.; Shen, L.; Huang, R.; Wang, H.; Pastore, J. P.; Yu, S. H.; Xiao, L.; Brock, J. D.; Zhuang, L.; Abruña, H. D. In Situ X-Ray Absorption Spectroscopy of a Synergistic Co-Mn Oxide Catalyst for the Oxygen Reduction Reaction. *J. Am. Chem. Soc.* **2019**, *141*, 1463−1466.

(22) Yang, Y.; Peng, H.; Xiong, Y.; Li, Q.; Lu, J.; Xiao, L.; DiSalvo, F. J.; Zhuang, L.; Abruña, H. D. High-Loading Composition-Tolerant Co−Mn Spinel Oxides with Performance beyond 1 W/Cm^2 in Alkaline Polymer Electrolyte Fuel Cells. *ACS Energy Lett.* **2019**, *4*, 1251−1257.

(23) Shibli, S. M. A.; Arun, P. S.; Raj, A. V. Exploration of Octahedrally Shaped $MnCo_2O_4$ Catalyst Particles for Visible Light Driven Photocatalytic Water Splitting Reaction. *RSC Adv.* **2015**, *5*, 19393−19399.

(24) Chen, P.; Xu, K.; Fang, Z.; Tong, Y.; Wu, J.; Lu, X.; Peng, X.; Ding, H.; Wu, C.; Xie, Y. Metallic Co_4N Porous Nanowire Arrays Activated by Surface Oxidation as Electrocatalysts for the Oxygen Evolution Reaction. *Angew. Chem., Int. Ed.* **2015**, *54*, 14710−14714.

(25) Luo, J.; Tian, X.; Zeng, J.; Li, Y.; Song, H.; Liao, S. Limitations and Improvement Strategies for Early-Transition-Metal Nitrides as Competitive Catalysts toward the Oxygen Reduction Reaction. *ACS Catal.* **2016**, *6*, 6165−6174.

(26) Varga, T.; Vásárhelyi, L.; Ballai, G.; Haspel, H.; Oszkó, A.; Kukovecz, Á.; Kónya, Z. Noble-Metal-Free Iron Nitride/Nitrogen-Doped Graphene Composite for the Oxygen Reduction Reaction. *ACS Omega* **2019**, *4*, 130−139.

(27) Tian, X.; Luo, J.; Nan, H.; Fu, Z.; Zeng, J.; Liao, S. Binary Transition Metal Nitrides with Enhanced Activity and Durability for

DOI: 10.1021/jacs.9b10809
J. Am. Chem. Soc. 2019, 141, 19241−19245

the Oxygen Reduction Reaction. *J. Mater. Chem. A* **2015**, *3*, 16801−16809.
(28) Zhang, H.; Liu, M.; Cheng, W.; Li, Y.; Zhou, W.; Su, H.; Zhao, X.; Yao, P.; Liu, Q. Metallic Ni_3/N Quantum Dots as a Synergistic Promoter for NiO Nanosheet toward Efficient Oxygen Reduction Electrocatalysis. *J. Phys. Chem. C* **2019**, *123*, 8633−8639.
(29) Wang, L.-C.; Liu, B.-H.; Su, C.-Y.; Liu, W.-S.; Kei, C.-C.; Wang, K.-W.; Perng, T.-P. Electronic Band Structure and Electrocatalytic Performance of Cu_3N Nanocrystals. *ACS Appl. Nano Mater.* **2018**, *1*, 3673−3681.
(30) Oda, K.; Yoshio, T.; Oda, K. Preparation of Co-N Films by Rf-Sputtering. *J. Mater. Sci.* **1987**, *22*, 2729−2733.
(31) Zhang, Y.; Ouyang, B.; Xu, J.; Jia, G.; Chen, S.; Rawat, R. S.; Fan, H. J. Rapid Synthesis of Cobalt Nitride Nanowires: Highly Efficient and Low-Cost Catalysts for Oxygen Evolution. *Angew. Chem., Int. Ed.* **2016**, *55*, 8670−8674.
(32) Zhu, X.; Jin, T.; Tian, C.; Lu, C.; Liu, X.; Zeng, M.; Zhuang, X.; Yang, S.; He, L.; Liu, H.; Dai, S. In Situ Coupling Strategy for the Preparation of FeCo Alloys and Co_4N Hybrid for Highly Efficient Oxygen Evolution. *Adv. Mater.* **2017**, *29*, 1704091.
(33) Meng, F.; Zhong, H.; Bao, D.; Yan, J.; Zhang, X. In Situ Coupling of Strung Co_4N and Intertwined N-C Fibers toward Free-Standing Bifunctional Cathode for Robust, Efficient, and Flexible Zn-Air Batteries. *J. Am. Chem. Soc.* **2016**, *138*, 10226−10231.
(34) Yoon, K. R.; Shin, K.; Park, J.; Cho, S. H.; Kim, C.; Jung, J. W.; Cheong, J. Y.; Byon, H. R.; Lee, H. M.; Kim, I. D. Brush-Like Cobalt Nitride Anchored Carbon Nanofiber Membrane: Current Collector-Catalyst Integrated Cathode for Long Cycle Li-O_2 Batteries. *ACS Nano* **2018**, *12*, 128−139.
(35) Liu, X.; Zang, W.; Guan, C.; Zhang, L.; Qian, Y.; Elshahawy, A. M.; Zhao, D.; Pennycook, S. J.; Wang, J. Ni-Doped Cobalt-Cobalt Nitride Heterostructure Arrays for High-Power Supercapacitors. *ACS Energy Lett.* **2018**, *3*, 2462−2469.
(36) Regan, T. J.; Ohldag, H.; Stamm, C.; Nolting, F.; Lüning, J.; Stöhr, J.; White, R. L. Chemical Effects at Metal/Oxide Interfaces Studied by x-Ray-Absorption Spectroscopy. *Phys. Rev. B: Condens. Matter Mater. Phys.* **2001**, *64*, 214422.
(37) de Groot, F. M. F.; Fuggle, J. C.; Thole, B. T.; Sawatzky, G. A. 2p X-Ray Absorption of 3d Transition-Metal Compounds: An Atomic Multiplet Description Including the Crystal Field. *Phys. Rev. B: Condens. Matter Mater. Phys.* **1990**, *42*, 5459−5468.
(38) Pandey, N.; Gupta, M.; Gupta, R.; Rajput, P.; Stahn, J. Structure and Magnetization of Co_4N Thin Film. *J. Magn. Magn. Mater.* **2018**, *448*, 274−277.
(39) Zhao, Y.; Feltes, T. E.; Regalbuto, J. R.; Meyer, R. J.; Klie, R. F. *In Situ* Electron Energy Loss Spectroscopy Study of Metallic Co and Co Oxides. *J. Appl. Phys.* **2010**, *108*, 063704.
(40) Fehlner, F. P. *Low Temperature Oxidation: The Role of Vitreous Oxides*; A Wiley-Interscience Publication, John Wiley & Sons: New York, 1986.
(41) Grunze, M.; Brundle, C. R.; Tománek, D. Adsorption and Decomposition of Ammonia on a W(110) Surface: Photoemission Fingerprinting and Interpretation of the Core Level Binding Energies Using the Equivalent Core Approximation. *Surf. Sci.* **1982**, *119*, 133−149.
(42) Egawa, C.; Naito, S.; Tamaru, K. Adsorption and Decomposition of Ammonia on W(100); XPS and UPS Studies. *Surf. Sci.* **1983**, *131*, 49−60.
(43) Stańczyk, K.; Dziembaj, R.; Piwowarska, Z.; Witkowski, S. Transformation of Nitrogen Structures in Carbonization of Model Compounds Determined by XPS. *Carbon* **1995**, *33*, 1383−1392.
(44) Davis, R. E.; Horvath, G. L.; Tobias, C. W. The Solubility and Diffusion Coefficient of Oxygen in Potassium Hydroxide Solutions. *Electrochim. Acta* **1967**, *12*, 287−297.
(45) Abroshan, H.; Bothra, P.; Back, S.; Kulkarni, A.; Nørskov, J. K.; Siahrostami, S. Ultrathin Cobalt Oxide Overlayer Promotes Catalytic Activity of Cobalt Nitride for the Oxygen Reduction Reaction. *J. Phys. Chem. C* **2018**, *122*, 4783−4791.
(46) Xiong, Y.; Yang, Y.; DiSalvo, F. J.; Abruña, H. D. Metal-Organic-Framework-Dervied Co-Fe Bimetallic Oxygen Reduction Electrocatalyst for Alkaline Fuel Cells. *J. Am. Chem. Soc.* **2019**, *141*, 10744−10750.
(47) Gewirth, A. A.; Varnell, J. A.; DiAscro, A. M. Nonprecious Metal Catalysts for Oxygen Reduction in Heterogeneous Aqueous Systems. *Chem. Rev.* **2018**, *118*, 2313−2339.

DOI: 10.1021/jacs.9b10809
J. Am. Chem. Soc. 2019, 141, 19241−19245